Progress In Electromagnetics Research M, Vol. 88, 145–157, 2020

Transverse Resolution in Microwave Imaging for Strip Objects Buried in a Half-Space Medium

Maria A. Maisto*, Raffaele Solimene, and Rocco Pierri

Abstract—In this paper we are concerned with a microwave imaging problem for a non-magnetic two-layered background medium, where objects are buried in the lower half-space, and the scattered field is collected in the upper one according to a multi-monostatic configuration. In particular, we are interested in estimating the achievable transverse resolution. As well known, range resolution mainly depends on the working frequency band whereas transverse resolution depends on the geometrical parameters of the configuration and is usually computed in correspondence to the highest (or even the average) adopted frequency. Determining transverse resolution is much more difficult, and closed form estimations have been actually found only for the case of unbounded observation domain. However, in real scattering scenarios, measurements have to be necessarily collected under an aspect limited setup. Therefore, in order to fill such a theoretical gap, here the focus is on the estimation of transverse resolution for bounded observation domains. To this end, we consider a single-frequency 2D scalar prototype configuration where the buried scattering object domain is represented by a strip parallel to the half-space interface. More in detail, we succeed in finding an analytical estimation of the transverse resolution which highlights the role of the configuration parameters as well as the dielectric permittivity of the lower half-space.

1. INTRODUCTION

Subsurface imaging entails dealing with an inverse scattering problem in which the targets are embedded within an inhomogeneous background medium. As such, it is relevant in a number of applicative contexts that range from non-destructive testing to geophysical prospecting, from buried-object detection to mine detection [1], etc.

As is well known, electromagnetic inverse scattering problems require the inversion of a nonlinear and ill-posed mathematical relationship. A number of nonlinear approaches that basically achieve inversion through optimisation procedures, both deterministic and stochastic [2–7], have been developed. However, these methods are in general computationally demanding and can suffer from the local minima problem [8].

If quantitative reconstructions are not required, the problem can be drastically simplified by linearising the scattering equations, for example using the Born approximation [9–15]. However, ill-posedness still requires adopting some regularisation procedure [16], which limits the achievable resolution. In this framework, determining the achievable resolution and how it depends on the configuration is of great importance since, having set the configuration, this allows to foresee the achievable performance during the imaging stage, or viceversa, and given the degree of accuracy to obtain in the reconstruction the configuration can be settled accordingly.

As is well known, range resolution mainly depends on the adopted frequency band [17, 18]. Instead, transverse resolution, usually estimated in correspondence to the highest (or even the average) adopted

Received 3 August 2019, Accepted 19 October 2019, Scheduled 15 January 2020

* Corresponding author: Maria Antonia Maisto (mariaantonia.maisto@unicampania.it).

The authors are with the Dipartimento di Ingegneria, Universitá della Campania, Luigi Vanvitelli, Aversa (Ce) 81031, Italy.

frequency, is much more difficult to determine (especially for near-field cases) since it depends on the geometrical parameters of the configuration and of course on the half-space medium dielectric permittivity. Literature on subsurface imaging, though extensive, is mainly devoted to discussing imaging algorithms. Indeed, transverse resolution is usually estimated by employing Fourier based arguments which ignore truncation effects (i.e., the measurement aperture is considered unbounded) [19]. As a result, for the aspect limited configuration, the estimated transverse resolution is incorrect and fails to capture the spatially varying behaviour that characterises the resolution for the near-zone configuration [14]. The estimation of the resolution for near-field configuration is also addressed in [17, 18, 20, 21]. However, those papers consider a homogeneous background medium. Moreover, in [17, 18] the resolution is estimated by basically using the classical far-field formula.

Previous discussion highlights the need to bridge the theoretical gap concerning transverse resolution estimation for aspect limited near-field cases. Accordingly, here the aim is to find an analytical estimation of transverse resolution for such cases. To this end, we consider a 2D scalar multi-monostatic single-frequency configuration where the buried scattering domain is a strip parallel to the half-space interface.

Since we are within a linear framework, transverse resolution estimation can be estimated as the width of the main beam of the reconstruction of a point-like target, i.e., the point-spread function (psf) of the imaging procedure. In general, the psf (and hence resolution) can depend on the imaging algorithm (or equivalently on the adopted regularisation scheme) and on the noise level. However, if evanescent waves are negligible [22], the singular values of the scattering operator exhibit a step-like behaviour. This behaviour entails that unless a very high signal-to-noise ratio (SNR) is available, one is forced to retain a fixed number of singular functions: the so-called number of degrees of freedom (NDF). Accordingly, the psf can be computed by a truncated singular value decomposition (TSVD) expansion. Moreover, the corresponding achievable resolution is weakly dependent on the noise and the adopted regularisation scheme, and mainly depends on the parameters of the configuration. However, for the problem at hand, the SVD of the scattering operator is not known in closed form, and hence, by this method, resolution cannot be estimated analytically. Therefore, in order to analytically estimate the achievable transverse resolution, we follow the approach developed in [20, 21]. Basically, the regularised inverse is approximated by the adjoint of the scattering operator once the scattered field has properly been filtered through a suitable weighting function. In particular, by this inversion scheme both the phase (as in standard migration schemes) and the amplitude of the propagator (involved in the scattering operator) are properly compensated. The obtained transverse resolution estimation highlights the role of the configuration parameters and captures the above mentioned spatially varying behaviour. Moreover, it very well matches the psf obtained by a numerical TSVD, which is used here as ground truth.

Finally, the paper also includes a comparison with the homogeneous free-space case in order to show how the half-space medium impacts on the resolution.

2. PROBLEM DESCRIPTION

The considered 2D scalar scattering problem is sketched in Fig. 1, and invariance is assumed along the y-axis. The background medium consists of two homogeneous non-magnetic (i.e., the magnetic permeability is everywhere the one of free-space μ_0) half-spaces separated by a planar interface at $z = 0$, with their dielectric permittivity and wave-numbers being ϵ_u, k_u for the upper half-space and ϵ_l, k_l for the lower one. In particular, the lower medium is considered electromagnetically denser than the upper one, that is $k_l > k_u$.

The unknown targets are embedded in the lower half-space and assumed to reside within the segment SD (i.e., the investigation domain) located at $z_s < 0$. The incident field is radiated by a y-polarized line source of unitary amplitude. The time dependence is assumed equal to e^{jwt} and omitted. The only y component of the scattered field is collected by exploiting a multi-monostatic measurement configuration, where the transmitting and receiving antennas are located at the same position in the upper half-space. The antenna system moves along the segment $OD = [-X_0, X_0]$ (i.e., the observation domain) of the x-axis located at the height $z_o > 0$ and parallel to SD.

Under the Born approximation, the contrast function χ and scattered field are linked through the

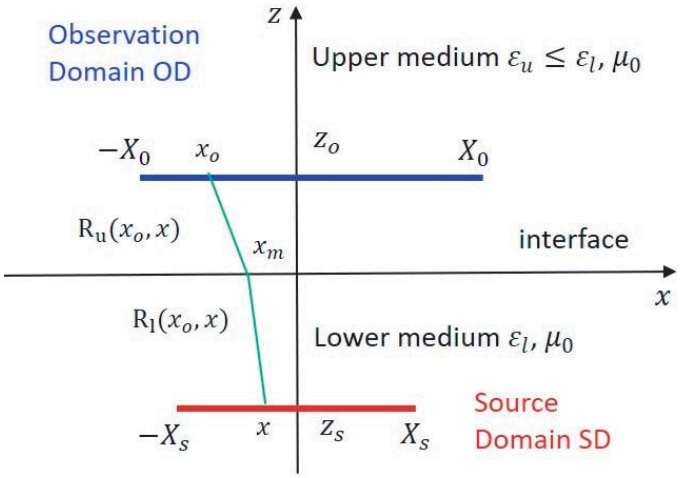

Figure 1. Geometry of the problem.

following scattering operator

$$\mathcal{A} : \chi \in L^2(SD) \rightarrow E \in L^2(OD) \tag{1}$$

where $L^2(SD)$ and $L^2(OD)$ represent the set of square integrable functions supported over SD and OD, respectively. The χ function is defined as $(\epsilon_s(\dot{}) - \epsilon_l)/\epsilon_l$, with $\epsilon_s(\dot{})$ being the dielectric permittivity of the unknown scatterer. The explicit form of the operator is given by

$$E(x_o) = k_l^2 \int_{SD} G^2(x_o, x, z_s)\chi(x)dx \quad x_o \in OD \tag{2}$$

with $G(\cdot)$ being the Green function pertinent to the two-layered background medium whose expression in terms of the Weyl expansion is

$$G(x_o, x, z_s) = \frac{i}{2\pi} \int_{-\infty}^{\infty} \hat{G}(k_x, z_o, z_s) e^{-jk_x(x_o - x)} dk_x \tag{3}$$

with

$$\begin{aligned} \hat{G}(k_x, z_o, z_s) &= \frac{1}{2}\tau(k_x) e^{jk_{zl}z_s} e^{-jk_{zu}z_o} \\ \tau(k_x) &= \frac{2}{k_{zl} + k_{zu}} \\ k_{zl} &= \begin{cases} \sqrt{k_l^2 - k_x^2} & \text{if} \quad k_x \leq k_l \\ -j\sqrt{k_x^2 - k_l^2} & \text{if} \quad k_x > k_l \end{cases} \end{aligned}$$

and

$$k_{zu} = \begin{cases} \sqrt{k_u^2 - k_x^2} & \text{if} \quad k_x \leq k_u \\ -j\sqrt{k_x^2 - k_u^2} & \text{if} \quad k_x > k_u \end{cases}$$

Note that the square in Eq. (2) takes into account the multi-monostatic measurement configuration. By considering z_o, $z_s > \lambda_l > \lambda_u$, the Green function in Eq. (3) can be approximated as [15]

$$G(x_o, x, z_s) \approx h(x_o, x, z_s) e^{-j\phi(x_o, x, z_s)} \tag{4}$$

where $h(x_o, x, z_s)$ takes into account the relevant amplitude factors, with $\phi(x_o, x.z_s) = k_u(R_u + R_l)$, $R_u = \sqrt{(x_o - x_m(x_o, x, z_s))^2 + z_o^2}$, $R_l = n\sqrt{(x_m(x_o, x, z_s) - x)^2 + z_s^2}$, $n = \sqrt{\epsilon_l/\epsilon_u}$ being the refractive index, and $x_m(x_o, x, z_s)$ is the refraction point at the half-space interface according to Snell's law

$$\frac{x_o - x_m}{\sqrt{(x_o - x_m)^2 + z_o^2}} = n\frac{x_m - x}{\sqrt{(x_m - x)^2 + z_s^2}} \tag{5}$$

The imaging problem consists in solving Eq. (2) for χ. In particular, in view of the linearity of the problem, the resolution can be estimated by considering the reconstruction of a point-like scatterer, which is the so-called point-spread function. More in detail, here, we adopt the classical Rayleigh's criterion, which consists in estimating the achievable resolution as the distance between the maximum and the first zero of the point-spread function of the imaging procedure. Note that this also represents the so-called two-point resolution, which is the distance between two point-like targets in order to be distinguishable in the reconstruction. Fig. 2 illustrates the meaning of resolution.

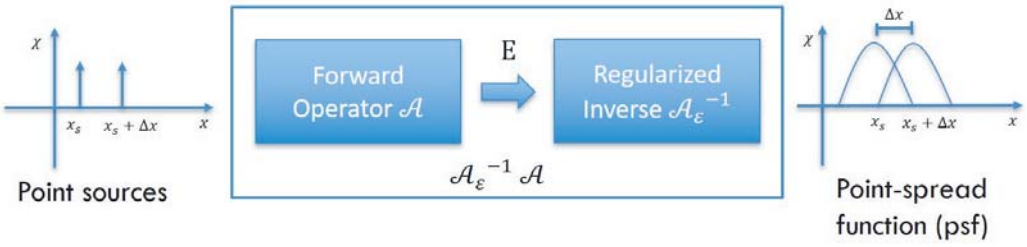

Figure 2. Graphical explanation of resolution.

By using the singular system $\{u_n, v_n, \sigma_n\}_{n=0}^{\infty}$ of the scattering operator, with u_ns and v_ns spanning $Dom(\mathcal{A})$ and $\bar{R}(\mathcal{A})$, respectively, the solution of Eq. (2) can be formally expressed as

$$\chi(x) = \sum_{n=0}^{\infty} \frac{\langle E + \mathcal{N}, v_n \rangle}{\sigma_n} u_n(x) \tag{6}$$

where $\langle \cdot, \cdot \rangle$ represents the scalar product in the field space, and $\mathcal{N}$ is the noise. Since $\mathcal{A}$ is compact, the inverse scattering problem is ill-posed [23]. Hence, regularisation is mandatory and the achievable resolution results limited. As a consequence, the reconstruction χ_R is a filtered version of the unknown χ, that is

$$\chi_R(x) = \int_{SD} psf(x, x')\chi(x')dx' \tag{7}$$

with the filtering kernel just given by the $psf(\cdot, \cdot)$. Accordingly, by studying the psf one gets insights not only on the two-point resolution but also on the filtering that the unknown undergoes during the reconstruction process. Therefore, estimating the resolution is basically a measure of the finest detail about the unknown that can be reconstructed.

A simple way to achieve regularisation is to truncate the singular value decomposition (TSVD) [16]. If ϵ is the noise dependent truncation level and N_ϵ the number of singular values above it, thenn by considering, in Eq. (6), a point-like target located at x' it yields the following psf expression

$$psf(x, x') = \sum_{n=0}^{N_\epsilon} u_n(x')u_n(x) \tag{8}$$

Equation (8) shows how the psf, and hence the resolution can be in general noise dependent. Indeed, this is particularly true when evanescent waves are relevant [22]. For the case at hand (see next sections), the singular values exhibit an abrupt exponential decay beyond a certain critical index. Hence, it is natural to identify such an index as the NDF of the problem. As a consequence, the point-spread function turns out to be weakly dependent on the signal to noise ratio (SNR), and the resolution mainly depends on the configuration parameters, which in turn determine the mentioned critical index.

We are not able, herein, to work out the relevant singular system. Hence, in order to obtain the point-spread function, we follow the same approach developed in [20, 21] where a weighted adjoint method is exploited. This procedure permits to directly approximate the point-spread function so that Eq. (8) (computed numerically) will be solely used as a benchmark in order to check the analytical estimation. The obtained point-spread function will be also used to estimate the NDF [21].

3. POINT-SPREAD FUNCTION ESTIMATION

As anticipated above, to obtain the reconstruction, we employ a weighted adjoint inversion scheme. Accordingly, the reconstruction is written as

$$\chi_R(x) = (\mathcal{A}^\dagger W(x,x_o)\mathcal{A}\chi)(x) = \int_{-X_s}^{X_s} \chi(x')dx' \times \int_{-X_0}^{X_0} W(x,x_o)h^{*2}(x_o,x)h^2(x_o,x')e^{2j[\phi(x_o,x)-\phi(x_o,x')]}dx_o \quad (9)$$

where, besides the adjoint operator kernel, one can recognise the weighting function $W(x,x_o)$. As is well known, inversion through the adjoint operator allows to get stable reconstructions, but such an inversion scheme is not a regularisation in the sense of Tichhonov [16]. Basically, this is because while the propagator phase is precisely compensated in correspondence to the target position, the amplitude term is not addressed properly. The weighing function aims at remedying such a lack. In particular, W must be chosen so that the corresponding point-spread function is as close as possible to a filtered version of a Dirac-delta function.

In order to proceed further in that direction and find the resolution, the idea is to recast $\mathcal{A}^\dagger W(x,x_o)\mathcal{A}$ as a Fourier type integral operator.

To this end, the Fundamental Theorem of Calculus (FTC) is used to express the phase term as

$$2\left[\phi(x_o,x)-\phi(x_o,x')\right] = 2\int_{x'}^{x} \frac{\partial\phi(x_o,p)}{\partial p}\,dp \quad (10)$$

Now, introduce the transformation $p = x'+\alpha(x-x')$ and replace the integration in p with the integration in α. Clearly α is an auxiliary integration variable that must range from 0 to 1 because p ranges from x' to x. Upon performing the aforesaid change of the integration variable, Eq. (10) is rewritten as

$$2\left[\phi(x_o,x)-\phi(x_o,x')\right] = (x-x')2\int_0^1 \left.\frac{\partial\phi(x_o,p)}{\partial p}\right|_{p=x'+\alpha(x-x')} d\alpha \quad (11)$$

Finally, by putting

$$w(x,x',x_o) = 2\int_0^1 \left.\frac{\partial\phi(x_o,p)}{\partial p}\right|_{p=x'+\alpha(x-x')} d\alpha \quad (12)$$

we obtain

$$2\left[\phi(x_o,x)-\phi(x_o,x')\right] = (x-x')w(x,x',x_o) \quad (13)$$

The function $w(x,x',x_o)$ is continuous and monotonic with respect to x_o (hence invertible) $\forall x,x'$. This allows to replace the integration in x_o with the integration in w. Then, by centring around zero the integration of w, we set

$$\Delta w(x,x',X_0) = \frac{w(x,x',-X_0)-w(x,x',X_0)}{2} \quad (14)$$

and

$$w_m(x,x',X_0) = \frac{w(x,x',-X_0)+w(x,x',X_0)}{2} \quad (15)$$

Note that because of Eq. (12), we have

$$w_m(x-x') = \left[\frac{w(x,x',-X_0)+w(x,x',X_0)}{2}\right](x-x') = (x-x')\int_0^1 \left.\frac{\partial\phi(-X_0,p)}{\partial p}\right|_{p=x'+\alpha(x-x')} d\alpha + (x-x')\int_0^1 \left.\frac{\partial\phi(X_0,p)}{\partial p}\right|_{p=x'+\alpha(x-x')} d\alpha \quad (16)$$

Then, by inserting in Eq. (16), Eq. (11) evaluated for $x_o = X_0$ and $x_o = -X_0$, we obtain

$$w_m(x-x') = \gamma(x)-\gamma(x') \quad (17)$$

with $\gamma(x) = [\phi(-X_0, x) + \phi(X_0, x)]$. Accordingly, Eq. (9) becomes

$$(\mathcal{A}^\dagger W \mathcal{A}\chi)(x) = \int_{-X_s}^{X_s} \chi(x') e^{j(\gamma(x)-\gamma(x'))} \int_{-\Delta w(x,x',X_0)}^{\Delta w(x,x',X_0)} H(\bar{w} + w_m, x, x') e^{j\bar{w}(x-x')} d\bar{w} dx' \tag{18}$$

with

$$H(w, x, x') = -W(x_o(w), x) h^{*2}(x_o(w), x) h^2(x_o(w), x') \frac{dx_o}{dw}$$

In particular, by comparing Eq. (18) with Eq. (7), one can identify the inner integral (i.e., the one with respect to $\bar{w}$) as the $psf_W(x, x')$, where subscript W is just a reminder that the weighted inversion scheme has been employed. In particular, the expected spatially varying behaviour of transverse resolution is evident since the spectral integration interval depends on x and x'.

In order to avoid unwanted "tapering" that can reduce resolution, the amplitude term H still needs to be compensated. To this end, we note that the leading order contribution of the integral in $\bar{w}$ of Eq. (18) occurs for $x - x' = 0$ [24]. Then, the amplitude factor can be approximated as $H(w, x, x') \approx H(w, x', x') = H(w, x')$, which helps us in the choice of the weighting function W. Indeed, the best we can do is to equalize the amplitude factor so that $H(w, \eta') = 1$. In view of the definition of $H(\cdot)$ and since at $x = x'$

$$w(x', x', x_o) = w(x', x_o) = 2\frac{\partial \phi(x_o, x')}{\partial x'} \tag{19}$$

and

$$\frac{dx_o}{d\bar{w}} = \frac{dw}{dx_o}^{-1} = \left[2\frac{\partial^2 \phi(x_o, x)}{\partial x_o \partial x'}\right]^{-1} \tag{20}$$

then

$$W(w, x') = 2\left|\frac{\partial^2 \phi(x_o, x)}{\partial x_o \partial x}\right| \frac{1}{|h^2(x_o, x)|^2} \tag{21}$$

Accordingly, Eq. (18) becomes

$$(\mathcal{A}^\dagger W \mathcal{A}\chi)(x) = \int_{-X_s}^{X_s} \chi(x') e^{j(\gamma(x)-\gamma(x'))} \int_{-\Delta w(x,x',X_0)}^{\Delta w(x,x',X_0)} e^{j\bar{w}(x-x')} d\bar{w} dx' \tag{22}$$

Now, by introducing the transformation

$$\eta(x) = [\phi(-X_0, x) - \phi(X_0, x)] \tag{23}$$

it can be shown, by following the same passages used for deriving Eq. (17), that

$$\Delta w(x, x', X_0)(x - x') = \eta(x) - \eta(x') \tag{24}$$

and hence Eq. (22) is rewritten as

$$(\mathcal{A}^\dagger W \mathcal{A}\chi)(\eta) = \int_{\eta'(-X_s)}^{\eta'(X_s)} \chi(\eta') 2e^{j(\gamma(\eta)-\gamma(\eta'))} \mathrm{sinc}(\eta - \eta') \Delta w \frac{dx'}{d\eta'} d\eta' \tag{25}$$

Finally, because of Eq. (19), $\Delta w = \left[\frac{d\eta'}{dx'}\right]$, and the following (sought after) expression for the point-spread function is obtained

$$psf_W(\eta, \eta') = 2e^{j(\gamma(\eta)-\gamma(\eta'))} \mathrm{sinc}(\eta - \eta') \tag{26}$$

It is interesting to remark that the spatially varying behaviour of the spectral interval, mentioned above, has been now transformed in the nonlinear link between the variables x and η, which clearly implies a spatially varying resolution. In particular, on denoting $x_m(-X_0, x, z_s) = f_1(x)$ and $x_m(X_0, x, z_s) = f_2(x)$, the explicit form of Eq. (23) is obtained as

$$\begin{aligned} \eta(x) \;=\; k_u \Bigg[& \sqrt{(X_0 + f_1(x))^2 + z_o^2} + n\sqrt{(f_1(x) - x)^2 + z_s^2} - \sqrt{(X_0 - f_2(x))^2 + z_o^2} \\ & - n\sqrt{(f_2(x) - x)^2 + z_s^2} \Bigg] \end{aligned} \tag{27}$$

Note that the analytical expression for $f_1(x)$ and $f_2(x)$ can be derived by solving Eq. (5) for $x_o = -X_0$ and $x_o = X_0$, respectively, for each $x \in SD$. However, for symmetry reasons $f_1(-x) = -f_2(x)$, and Eq. (27) can be rewritten as

$$\eta(x) = k_u \Bigg[\sqrt{(X_0 + f_1(x))^2 + z_o^2} + n\sqrt{(f_1(x) - x)^2 + z_s^2} - \sqrt{(X_0 + f_1(-x))^2 + z_o^2} - n\sqrt{(f_1(-x) + x)^2 + z_s^2} \Bigg] \tag{28}$$

This makes clear that $\eta(x)$ is an odd function of x, and hence, $\eta(X_s) = -\eta(-X_s)$. Moreover, only the calculation of $f_1(x)$ is required. The explicit expression of $f_1(x)$ is given in the appendix.

In order to check the theoretical findings, the psf_W returned by Eq. (26) has been compared with the psf obtained through Eq. (8), the latter obtained by numerically computing the singular system of $\mathcal{A}$ and by retaining in Eq. (8) the singular functions corresponding to the singular values preceding the abrupt decay (see next discussion on NDF). The simulations show an excellent agreement between psf_W and psf. As a representative example, here we report the case shown in Fig. 3, in which the upper half-space has been considered as the free-space, so that $k_u = k_0$, $\epsilon_u = \epsilon_0$ and $\lambda_u = \lambda_0$, whereas the lower half-space has $\epsilon_l = \epsilon_r \epsilon_0$. This assumption will be kept in all of the following examples. As can be appreciated, the two functions overlap very well; accordingly, it can be concluded that Eq. (26) works very well and can be used to estimate the achievable resolution.

4. RESOLUTION AND NDF ESTIMATION

As shown in the previous section, psf_W returns a good estimation of psf. Hence, it can be used to estimate the transverse resolution. By applying the Rayleigh's criterion to Eq. (26), the achievable resolution can be estimated as the width of main-beam of the point-spread function. Accordingly, it is immediately seen that, in the η variable, resolution is

$$\Delta\eta = \pi \tag{29}$$

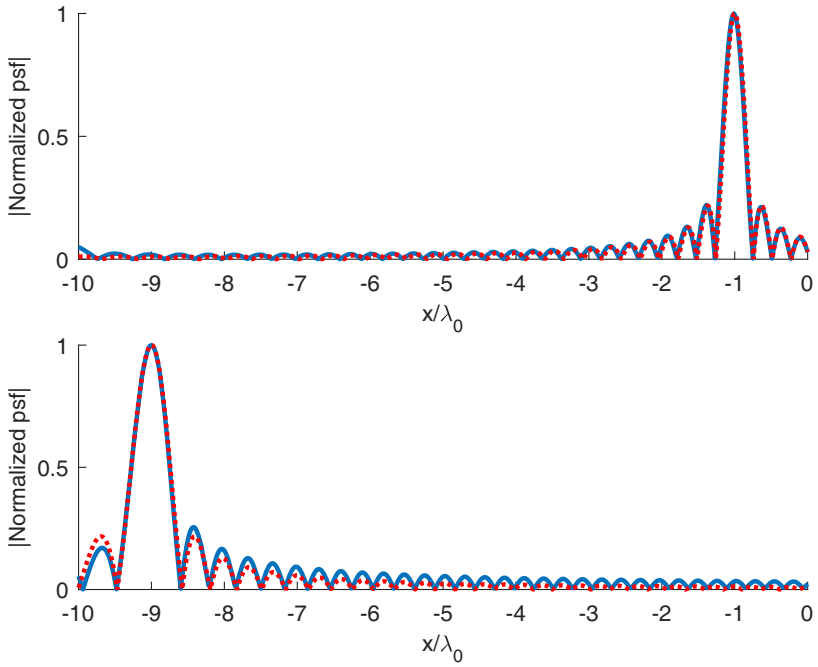

Figure 3. Normalized point spread functions' amplitudes for $\epsilon_r = 9$, $a = 10\lambda_0$, $X_0 = 9.5\lambda_0$, $z_1 = -5\lambda_0$ and $z_o = 2\lambda_0$. The blue lines refer to psf whereas the dotted red ones to psf_W. In the top panel the point scatterer is located at $-1\lambda_0$ and in the bottom at $-9\lambda_0$.

which, in terms of the x variable, reads as

$$\eta(x+\Delta x)-\eta(x)=\pi \tag{30}$$

In order to explicitly get the resolution in x, Eq. (30) should be solved for Δx. However, unlike the case of homogeneous medium [20], this does not appear as an easy task. Nonetheless, that equation links, even if implicitly (i.e., as an implicit function), the configuration parameters and Δx. Therefore, it allows to foresee the achievable resolution, once the configuration has been set, without running the reconstruction procedure. Moreover, some important features can be directly deduced by inspection: as we already mentioned above, since x and η are linked through a nonlinear relationship, Δx is spatially varying [25]. This indeed could have already been observed from Fig. 3 since the main-beam width of the psf changes with the positions of the point-like target.

An explicit but approximate expression for Δx can be obtained by truncating the Taylor series of $\eta(x+\Delta x)$ at the first term. By doing so it yields

$$\begin{aligned}\Delta x &\approx \frac{\pi}{\frac{d\eta}{dx}} \\ &= \frac{\lambda_u}{\left\{\begin{array}{l} 2\dfrac{(X_0+f_1(x))}{\sqrt{(X_0+f_1(x))^2+z_o^2}}f_1'(x)+n\dfrac{(f_1(x)-x)}{\sqrt{(f_1(x)-x)^2+z_s^2}}[f_1'(x)-1] \\ -\dfrac{(X_0+f_1(-x))}{\sqrt{(X_0+f_1(-x))^2+z_o^2}}f_1'(-x)-n\dfrac{(f_1(-x)+x)}{\sqrt{(f_1(-x)+x)^2+z_s^2}}[f_1'(-x)+1] \end{array}\right\}}\end{aligned} \tag{31}$$

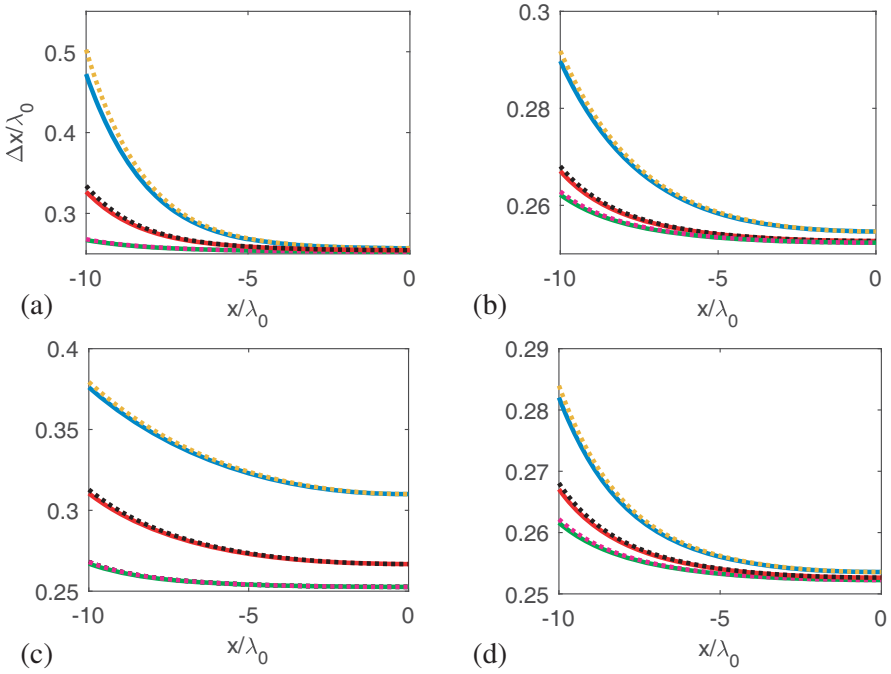

Figure 4. Comparison between Δx (solid lines) and the one returned by (31) (dotted lines) for different values of the geometrical parameters. (a) $n=3$, $z_s=-5\lambda_0$ and $z_o=2\lambda_0$ while $X_0=10\lambda_0$ (blue and yellow lines), $X_0=12\lambda_0$ (red and black lines) and $X_0=15\lambda_0$ (green and violet lines); (b) $X_0=15\lambda_0$, $z_s=-5\lambda_0$ and $z_o=2\lambda_0$ while $n=\sqrt{2}$ (blue and yellow lines), $n=3$ (red and black lines) and $n=6$ (green and violet lines); (c) $n=3$, $z_s=-5\lambda_0$ and $X_0=15\lambda_0$ while $z_o=10\lambda_0$ (blue and yellow lines), $z_o=5\lambda_0$ (red and black lines) and $z_o=2\lambda_0$ (green and violet lines); (d) $n=3$, $z_0=5\lambda_0$ and $X_0=15\lambda_0$ while $z_s=-10\lambda_0$ (blue and yellow lines), $z_s=-5\lambda_0$ (red and black lines) and $z_s=-2\lambda_0$ (green and violet lines).

with f_1' being the derivative of f_1 with respect to x. Obviously, Eq. (31) becomes more accurate as Δx decreases.

Figure 4 shows the comparison between Δx and the one returned by Eq. (31) (dotted lines) as the configuration parameters vary. As can be seen, Δx is spatially varying and gets worse when x moves toward the edge of SD. Also, such a spatially varying behaviour becomes more marked when $z_o - z_1$ increases or X_0 and n decrease. Moreover, Eq. (31) returns an excellent estimation of Δx. This behaviour of the resolution can be more easily explained by assuming X_0 large so that $f_1(x) \simeq x + \frac{z_s}{\sqrt{n^2-1}}$, and Eq. (31) is simplified as

$$\Delta x \simeq \frac{\lambda_u}{2\left[\dfrac{(\bar{X}_0 + x)}{\sqrt{(\bar{X}_0 + x)^2 + z_o^2}} + \dfrac{(\bar{X}_0 - x)}{\sqrt{(\bar{X}_0 - x)^2 + z_o^2}}\right]} = \frac{\lambda_u}{2(\sin\theta_r - \sin\theta_l)} \tag{32}$$

with $\bar{X}_0 = X_0 + \frac{z_s}{\sqrt{n^2-1}}$ being the equivalent measurement aperture and

$$\sin\theta_r = \frac{(\bar{X}_0 - x)}{\sqrt{(\bar{X}_0 - x)^2 + z_o^2}}$$

and

$$\sin\theta_l = -\frac{(\bar{X}_0 + x)}{\sqrt{(\bar{X}_0 + x)^2 + z_o^2}}$$

Firstly, Eq. (32) clearly shows that as X_0 increases, Δx tends to become constant. Therefore, the nonuniform behaviour of the resolution is essential due to truncation effects (i.e., limited observation

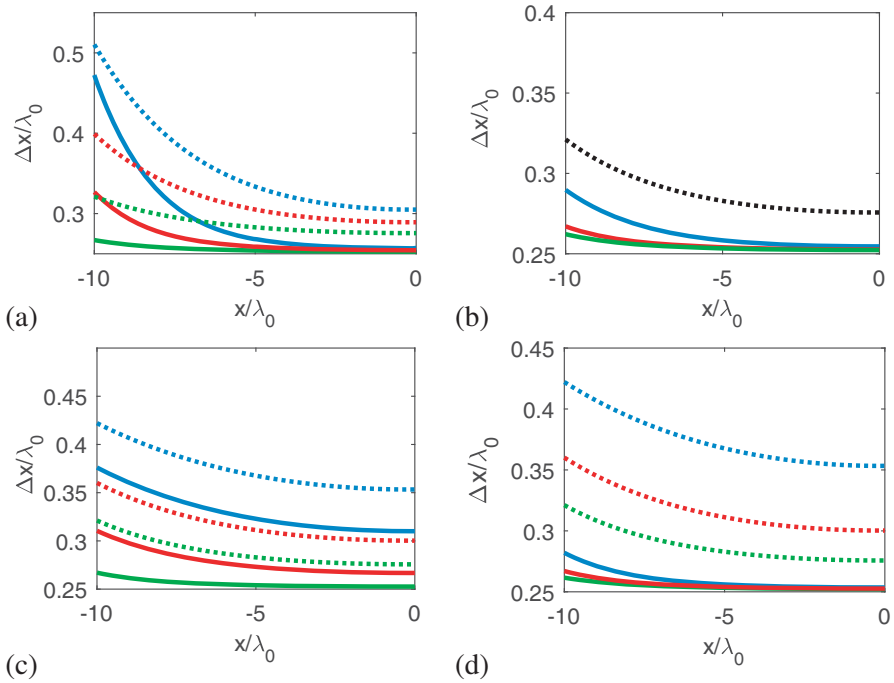

Figure 5. Comparison between Δx (solid lines) and Δx_h (dotted lines) for different values of the geometrical parameters. (a) $n = 3$, $z_s = -5\lambda_0$ and $z_o = 2\lambda_0$ while $X_0 = 10\lambda_0$ (blue lines), $X_0 = 12\lambda_0$ (red lines) and $X_0 = 15\lambda_0$ (green lines); (b) $X_0 = 15\lambda_0$, $z_s = -5\lambda_0$ and $z_o = 2\lambda_0$ while $n = \sqrt{2}$ (blue line), $n = 3$ (red line) and $n = 6$ (green line), the only black dotted-line refers to the homogeneous case; (c) $n = 3$, $z_s = -5\lambda_0$ and $X_0 = 15\lambda_0$ while $z_o = 10\lambda_0$ (blue lines), $z_o = 5\lambda_0$ (red lines) and $z_o = 2\lambda_0$ (green lines); (d) $n = 3$, $z_0 = 5\lambda_0$ and $X_0 = 15\lambda_0$ while $z_s = -10\lambda_0$ (blue lines), $z_s = -5\lambda_0$ (red lines) and $z_s = -2\lambda_0$ (green lines).

domain). In particular, Δx approaches $\lambda_u/4$ when $X_0 \to \infty$ (see Fig. 4(a)), which coincides with the estimation reported in [19] where an unbounded observation domain was considered.

Secondly, since in Eq. (32) z_s is divided by $\sqrt{n^2-1}$, the resolution will be more sensitive to z_o than z_s when n increases. This can be actually appreciated by comparing Figs. 4(c) and 4(d). More in general, Eq. (32) highlights how the resolution depends on the angular sector subtended by the measurement aperture. Since the latter depends on x, the resolution is spatially varying (as shown above). Moreover, that angular sector enlarges when X_0 and/or z_0 and/or z_s and/or n increase; this of course qualitatively justifies the theoretical results reported in Fig. 4.

At this juncture, in order to appreciate the role of the half-space scenario, it is interesting to compare the obtained resolution with the one of the homogeneous medium, Δx_h, (whose analytical expression has been derived in [20]). This comparison is shown in Fig. 5, where Δx (solid line) and Δx_h (dotted line) are reported for different parameters of the configuration. As can be appreciated, having fixed the configuration parameters, Δx is always lower than Δx_h. This entails that the interface improves the resolution (when OD is bounded indeed).

Finally, we switch to consider the NDF estimation. As mentioned above, the NDF is the number of significant singular values. However, since here the singular system is not known in closed form, borrowing from optics [26], the NDF is estimated by counting how many resolvable point-spread functions are required to fill the investigation domain. This approach can be conveniently worked out in the η domain, where the investigation domain is $[-\eta(X_s), \eta(X_s)]$. Accordingly, we obtain

$$\mathrm{NDF} = 2\frac{\eta(X_s)}{\Delta\eta} \tag{33}$$

In particular, since Eq. (33) does not in general return an integer value, and the NDF is estimated as the lowest integer which is greater than Eq. (33). In Fig. 6, some examples are reported to show the accuracy of Eq. (33). In particular, in that figure the singular value behaviour is reported for different

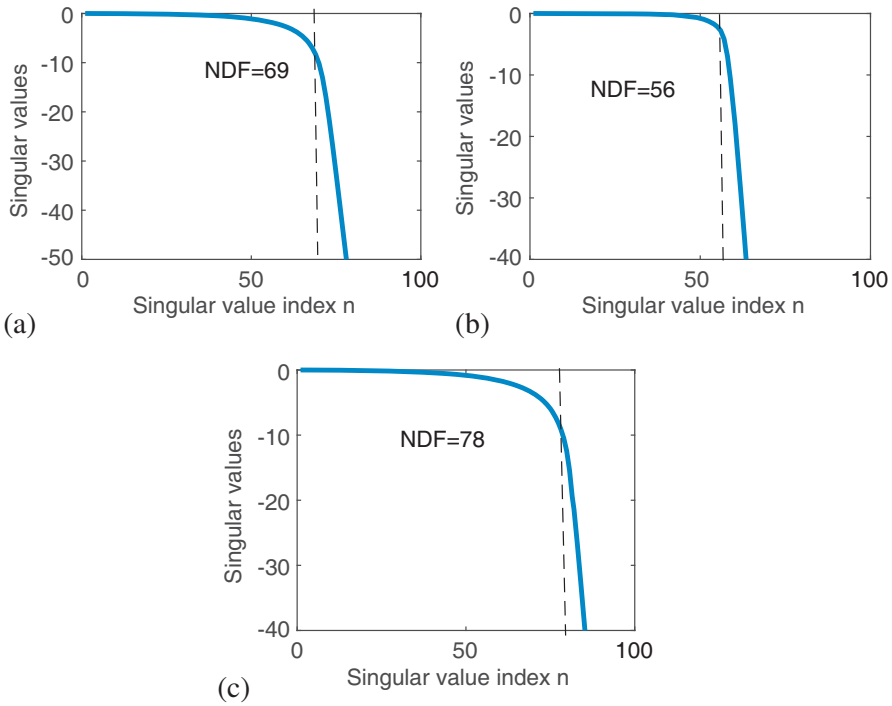

Figure 6. Normalized singular values of $\mathcal{A}$ for (a) $n = 3$ $a = 10\lambda_0$, $X_0 = 10\lambda_0$, $z_1 = -5\lambda_0$ and $z_o = 2\lambda_0$, (b) $n = \sqrt{3}$ $a = 10\lambda_0$, $X_0 = 10\lambda_0$, $z_1 = -5\lambda_0$ and $z_o = 5\lambda_0$, (c) $n = 2$ $a = 10\lambda_0$, $X_0 = 15\lambda_0$, $z_1 = -\lambda_0$ and $z_o = 2\lambda_0$. The dashed black line indicates the location of the knee. In each figure the values of NDF estimated by (33) are provided.

configurations along with vertical lines which mark the estimation returned by Eq. (33). As anticipated, the singular values actually exhibit a nearly step-like behaviour, and Eq. (33) returns a good estimation where the abrupt decay starts.

5. CONCLUSION

In this paper a linear inverse scattering problem for an inhomogeneous two-layered background medium has been addressed. In particular, in order to keep notation simple, a scalar two dimensional configuration has been addressed, where the investigation and observation domains are parallel bounded strips separated by a distance greater than the wavelength. In particular, a multi-monostatic measurement configuration has been considered.

The focus in this paper is to estimate the achievable transverse resolution and to highlight its dependence on the configuration parameters. To this end, by exploiting the approach developed in [20, 21], we find an expression for the psf, then, according to the Raylegth's criterion, an analytical estimation of the resolution. It is shown that because of the aspect limited configuration, transverse resolution is spatially varying and positively affected by the half-space scenario.

As remarked above, the obtained results hold as long as the singular values exhibit a step-like behaviour (unless unfeasible SNR is available). This condition basically rules out the cases where evanescent waves are relevant. In such cases, a different technique, as in [22], can be used.

ACKNOWLEDGMENT

The authors kindly thank Giuseppina Nuzzo for proofreading the manuscript.

APPENDIX A.

In this appendix, an analytical expression for $f_1(x)$ is derived. The function $f_1(x)$ solves Eq. (5) for $x_o = -X_0$, so

$$\frac{-X_0 - f_1(x)}{\sqrt{(X_0 + f_1(x))^2 + z_o^2}} = n\frac{f_1(x) - x}{\sqrt{(f_1(x) - x)^2 + z_s^2}} \tag{A1}$$

for each $x \in SD$. Equation (34) is equivalent to solving the following forth degree equation

$$af_1^4 + bf_1^3 + cf_1^2 + df_1 + e = 0 \tag{A2}$$

with

$$\begin{aligned} a &= (1 - n^2) \\ b &= -2(1 - n^2)(x - X_0) \\ c &= (X_0^2 + x^2 - 4X_0x)(1 - n^2) + z_1^2 - n^2 z_o^2 \\ d &= -2((xX_0^2 - X_0x^2)(1 - n^2) - X_0 z_1^2 - n^2 z_o^2 x) \\ e &= X_0^2 x^2 (1 - n^2) + z_1^2 X_0^2 - n^2 z_o^2 x^2; \end{aligned}$$

For each $x \in SD$, four solutions to Eq. (35) can be obtained, given by

$$\begin{aligned} f_1^a(x) &= -\frac{b}{4a} - S + 1/2\sqrt{-4S^2 - 2p + q/S} \\ f_1^b(x) &= -\frac{b}{4a} - S - 1/2\sqrt{-4S^2 - 2p + q/S} \\ f_1^c(x) &= -\frac{b}{4a} + S + 1/2\sqrt{-4S^2 - 2p - q/S} \\ f_1^d(x) &= -\frac{b}{4a} + S - 1/2\sqrt{-4S^2 - 2p - q/S} \end{aligned} \tag{A3}$$

with

$$\begin{aligned} p &= \frac{8ac - 3b^2}{8a^2} \\ q &= \frac{b^3 - 4abc + 8a^2 d}{8a^3} \\ S &= \frac{1}{2}\sqrt{-\frac{2}{3}p + \frac{1}{3a}\left(Q + \frac{\Delta_o}{Q}\right)} \\ Q &= \left(\frac{\Delta_1 + \sqrt{\Delta_1^2 - 4\Delta_0^3}}{2}\right)^{1/3} \\ \Delta_0 &= c^2 - 3bd + 12ae \\ \Delta_1 &= 2c^3 - 9bcd + 27b^2 e + 27ad^2 - 72ace \end{aligned}$$

However, only one of them fulfils Eq. (34). When $X_0 \to \infty$, Eq. (34) is simplified in

$$-1 = n\frac{f_1(x) - x}{\sqrt{(f_1(x) - x)^2 + z_s^2}} \tag{A4}$$

whose solution becomes

$$f_1(x) = x + \frac{z_s}{\sqrt{n^2 - 1}} \tag{A5}$$

REFERENCES

1. Daniels, D. J., *Ground Penetrating Radar*, Wiley Online Library, 2005.
2. Pastorino, M., "Stochastic optimization methods applied to microwave imaging: A review," *IEEE Trans. Antennas Propag.*, Vol. 55, No. 3, 538–548, Mar. 2007.
3. Chen, X., K.-M. Huang, and X.-B. Xu, "Microwave imaging of buried inhomogeneous objects using parallel genetic algorithm combined with FDTD method," *Progress In Electromagnetics Research*, Vol. 53, 283–298, 2005.
4. Hajebi, M., A. Tavakoli, and A. Hoorfar, "Frequency domain inverse profiling of buried dielectric elliptical-cylindrical objects using evolutionary programming," *IEEE Geosci. Remote Sens. Lett.*, Vol. 15, No. 4, 503–507, Apr. 2018.
5. Sallucci, M., L. Poli, N. Anselmi, and A. Massa, "Multifrequency particle swarm optimization for enhanced multiresolution GPR microwave imaging," *IEEE Trans. Geosci. Remote Sensing*, Vol. 55, No. 3, 1305–1317, 2017.
6. Kamilov, U. S., D. Liu, H. Mansour, and P. T. Boufounos, "A recursive born approach to nonlinear inverse scattering," *IEEE Signal Process. Lett.*, Vol. 23, No. 8, 1052–1056, 2016.
7. Yu, Y., T. Yu, and L. Carin, "Three-dimensional inverse scattering of a dielectric target embedded in a lossy half-space," *IEEE Trans. Geosci. Remote Sensing*, Vol. 42, No. 5, 957–973, 2004.
8. Isernia, T., V. Pascazio, and R. Pierri, "On the local minima in a tomographic imaging technique," *IEEE Trans. Geosci. Remote Sensing*, Vol. 39, No. 7, 1596–1607, 2001.
9. Dong, Q. and C. M. Rappaport, "Microwave subsurface imaging using direct finite-difference frequency-domain-based inversion," *IEEE Trans. Geosci. Remote Sensing*, Vol. 47, No. 11, 3664–3670, 2009.
10. Cui, T. J. and W. C. Chew, "Novel diffraction tomographic algorithm for imaging two-dimensional targets buried under a lossy earth," *IEEE Trans. Geosci. Remote Sensing*, Vol. 38, No. 4, 2033–2041, 2000.
11. Sun, Y., L. Qu, S. Zhang, and Y. Yin, "MT-BCS-based two-dimensional diffraction tomographic GPR imaging algorithm with multivie multistatic configuration," *IEEE Geosci. Remote Sens. Lett.*, Vol. 13, No. 6, 831–835, 2016.

12. Qu, L., Y. Yin, Y. Sun, and L. Zhang, "Diffraction tomographic ground-penetrating radar multibistatic imaging algorithm with compressive frequency measurements," *IEEE Geosci. Remote Sens. Lett.*, Vol. 12, No. 10, 2011–2015, 2015.
13. Hansen, T. B. and P. M. Johansen, "Inversion scheme for ground penetrating radar that takes into account the planar air soil interface," *IEEE Trans. Geosci. Remote Sensing*, Vol. 38, No. 1, 496–506, 2000.
14. Leone, G. and F. Soldovieri, "Analysis of the distorted born approximation for subsurface reconstruction: Truncation and uncertainties effects," *IEEE Trans. Geosci. Remote Sensing*, Vol. 41, No. 1, 66–74, 2003.
15. Fortuny-Guasch, J., "A novel 3-D subsurface radar imaging technique," *IEEE Trans. Geosci. Remote Sensing*, Vol. 40, No. 2, 443–452, 2002.
16. Bertero, M., "Linear inverse and ill-posed problems," *Adv. Electron. Electron Phys.*, Vol. 75, 1–120, 1989.
17. Soumekh, M., "A system model and inversion for synthetic aperture radar imaging," *IEEE Transactions on Image Processing*, Vol. 1, No. 1, 64–76, 1992.
18. Lopez-Sanchez, J. M. and J. Fortuny-Guasch, "3-D radar imaging using range migration techniques," *IEEE Trans. Antennas Propag.*, Vol. 48, No. 5, 728–737, 2000.
19. Cui, T. J., W. C. Chew, X. X. Yin, and W. Hong, "Study of resolution and super resolution in electromagnetic imaging for half-space problems," *IEEE Trans. Antennas Propag.*, Vol. 52, No. 6, 1398–1411, 2004.
20. Maisto, M. A., R. Solimene, and R. Pierri, "Resolution limits in inverse source problem beyond the Fresnel zone," *J. Opt. Soc. Am. A*, Vol. 36, No. 5, 826–833, 2019.
21. Maisto, M. A., R. Solimene, and R. Pierri, "Depth resolution in strip current reconstructions in near non-reactive zone," *J. Opt. Soc. Am. A*, Vol. 36, No. 6, 975–982, 2019.
22. Solimene, R., M. A. Maisto, and R. Pierri, "Inverse source in near field: The case of strip current," *J. Opt. Soc. Am. A*, Vol. 35, 755–763, 2018.
23. Tikhonov, A. N. and V. I. Arsenine, *Solution to Ill-posed Problems*, Halstead, 1977.
24. Cheney, M. and R. J. Bonneau, "Imaging that exploits multipath scattering from point scatterers," *Inverse Problems*, Vol. 20, 1691–1711, 2004.
25. Maisto, M. A., R. Solimene, and R. Pierri, "Sampling approach for singular system computation of a radiation operator," *J. Opt. Soc. Am. A*, Vol. 36, 353–361, 2019.
26. Gabor, D., "Light and information," *Progress in Optics*, E. Wolf, ed., Vol. 1, 109–153, North-Holland, Amsterdam, The Netherlands, 1961.